ELSEVIER

Solid State Ionics 131 (2000) 165–174

SOLID STATE IONICS

www.elsevier.com/locate/ssi

Potentiometrical investigations of nanocrystalline copper

Ch.P. Gräf, U. Heim, G. Schwitzgebel*

FB11.3 Physical Chemistry, Saarland University, 66041 Saarbrücken, Germany

Received 3 February 1999; received in revised form 5 May 1999; accepted 18 May 1999

Abstract

Various samples of nanocrystalline copper have been investigated as electrodes in acid $CuSO_4$ solutions, with the objective of examining growth and relaxation processes by studying the time dependence of the potential E. During the dissolution of Cu_2O the disproportionation of Cu^+ ions and the formation of nanocrystalline copper was detected in the $E(t)$ curve. A simple model for estimating the surface relaxation according to the Gibbs–Wulff theorem was applied to crystals with shapes varying between cube and octahedron. When the edge atoms are included in the energetic calculations, the excess surface energy becomes dependent on the size of the crystals. Surface relaxation then interferes with crystal growing. In agreement with these results, no separate time region of relaxation could be found for the $E(t)$ of nanocrystalline copper. It was shown that the accurate measurement of electrode potentials of copper requires attention to the specific electrochemical properties of copper, above all its extreme sensitivity to O_2 traces. A simple procedure has been developed for trapping O_2 in the cell and monitoring its absence electrochemically.

Keywords: Nanocrystalline copper electrodes; Cu growth and relaxation; Surface energy calculation

1. Introduction

The surface Gibbs energy of small particles increases with decreasing diameter for a constant amount of substance. This excess free energy, ΔG_{GT}^{ex}, is the driving force for recrystallization of the growing of particles at the expense of smaller ones. The degree of the non-equilibrium state can be determined by ΔG_{GT}^{ex}, e.g.: in the case of small liquid droplets as the excess vapour pressure (Gibbs–Thomson) and in the case of small solid particles or nanocrystalline samples in contact with appropriate ionic conductors by measuring the excess EMF, ΔE^{ex} [1–4]. In these techniques there is an active exchange of atoms or molecules between the liquid and the gas phase or of atoms or ions between the solid and ion-conducting phase. This means that the local exchange equilibrium, and thus the measurement, is not or not markedly influenced by the global non-equilibrium.

Another type of non-equilibrium (ΔG_{GW}^{ex}) has to be taken into account in the case of crystals. The Gibbs–Wulff theorem states that the equilibrium shape of a free crystal is characterized by a minimum of free surface energy, which requires constancy of the fractions σ_i/h_i for all faces of the crystal (σ_i: specific free surface energy of face i; h_i: vertical distance from the Wulff centre). Faces of different σ_i of a metal crystal should exhibit different electrode

*Corresponding author. Tel.: +49-681-302-2913; fax: +49-681-302-4833.

E-mail address: g.schwitzgebel@rz.uni-sb.de (G. Schwitzgebel)

0167-2738/00/$ – see front matter
PII: S0167-2738(00)00631-7

potentials, E_i, when in electrochemical exchange with a ion conducting phase. But this has never been proved unequivocally and probably it cannot be proved, because no defined reversible electrode potential exists on a defect-free face of a single crystal of macroscopic dimensions ($>100\ \mu m^2$) [5]. The measurement process itself is based on the presence of defects – ad-atoms, steps, kinks and screw dislocations – but there is no guarantee that new face types do not appear when steps degenerate.

A better chance for indirect evidence of E_i differences can be expected from investigations of nanocrystalline metals, which are normally prepared in non-equilibrium shapes. Since ΔG^{ex}_{GW} like ΔG^{ex}_{GT} is inversely proportional to the particle diameter (Section 2.3), differences in E_i will be magnified according to the same proportionality. The fraction of edge atoms increases even more greatly, so that the measuring process is facilitated. Thus, the process of equilibration of the shape of crystals, which we call surface relaxation, is in principle superimposed on the growth process and it is an interesting question, if it can be detected by EMF or other phenomenological measurements, e.g. calorimetry [6,7].

The literature on recrystallization in contact with a neighbouring phase only seldom refers the Ostwald ripening [8]. One example of a quantitative time law of EMF change has been published [1], but there are more examples of qualitative observations [9–11]. Relaxation under the influence of stored excess free energy of strain, ΔG^{ex}_s, is a general phenomenon in solid state science, which has often been supposed to be also detectable and determinable potentiometrically [13–15].

Kinetic laws of relaxation have not been studied by EMF techniques hitherto. Some features of $\Delta E^{ex}(t)$ curves in our previous work on nanocrystalline copper (Cu_{nc}) [12] seemed to suggest relaxation effects. However, because of the peculiarities of the two-step electrode reaction of Cu and its extreme sensitivity against O_2, other interpretations must be taken into account. Therefore one of the objectives of this work was to scrutinize $\Delta E^{ex}(t)$ curves. The other was to treat surface relaxation from a very simplified point of view, in order to foresee how this type of relaxation could proceed.

2. Theory

2.1. Excess EMF of nanocrystalline metals

The Gibbs energy change of a chemical reaction, $\Delta_R G$, can be determined in a electrochemical cell, if this reaction is the cell reaction and if the electrode reactions with the electrolyte are reversible.

$$\Delta_R G = -z_e F\,\Delta E \tag{1}$$

In the specific cell,

$$M_{nc}/\text{solution with } M^{z+}/M_{mc}, \tag{2}$$

the metal in its microcrystalline state M_{mc} is in equilibrium with metal ions M^{z+},

$$M^{z+} + z_+ e^- = M_{mc}\ \text{(right side)} \tag{3}$$

(z_+: charge number). A similar equilibrium is supposed for the nanocrystalline metal M_{nc},

$$M^{z+} + z_+ e^- = M_{nc}\ \text{(left side)} \tag{4}$$

so that the cell reaction is given by

$$M_{nc} \rightarrow M_{mc} \tag{5}$$

and its EMF by

$$\Delta E^{ex} = E_{mc} - E_{nc}. \tag{6}$$

With Eq. (1) one obtains (F: Faraday constant)

$$-\Delta_R G = \Delta G^{ex} = z_e F\,\Delta E^{ex}. \tag{7}$$

In general ΔG^{ex} can be made up from different non-equilibrium contributions.

$$\Delta_R G^{ex} = \Delta G^{ex}_{GT} + \Delta G^{ex}_s + \Delta G^{ex}_{GW} \tag{8}$$

A generalized Gibbs–Thomson equation,

$$\Delta G_{GT} = g\,\sigma\,V_M/\bar{r} \tag{9}$$

($\bar{r}$: mean radius; σ: specific interfacial energy; V_M: molar volume of M; g: geometrical factor of the order of 1, describing the shape of the particles) is valid for the excess surface free energy ΔG^{ex}_{GT} [16]. The excess free energy of strain ΔG^{ex}_s has been calculated using the micro strain ϵ and mechanical stress laws [3,15] and for ΔG_{GW} an exemplary estimation will be given below (Section 2.3).

2.2. Grain growth

An increase of $\bar{r}$, i.e. grain growth, lowers the Gibbs energy ΔG^{ex}_{GT} of an assembly of crystals. The literature on this phenomenon is enormous [17], but one must distinguish between several types of growth. The growth of M_{nc} crystals in contact with a solution, which exchanges ions with the metal, is more than one order of magnitude faster than intrinsic grain growth [3]. Furthermore, this contact growth may proceed conservatively, i.e. all material which dissolves (from smaller crystals) is deposited on bigger ones, or non-conservatively, when material is lost into the solution by corrosion. All forced growth processes, induced by electrochemical deposition techniques [18], are also non-conservative.

The early results of Wagner [8] on contact growth of free spherical particles (Ostwald ripening) have been confirmed for surface layers [19]. Diffusion control of the elementary steps leads to

$$\bar{r}(t) = r_0 (1 - \gamma_d t)^{-1/3} \tag{10}$$

and reaction control to

$$\bar{r}(t) = r_0 (1 - \gamma_r t)^{-1/2} \tag{11}$$

where γ_i contains informations about the grain size distribution. With different meanings of γ_i the time laws of Eqs. (10) and (11) can also be derived in the case of non-conservative growth. But this condition has not yet been treated exhaustively and other time laws may exist [19].

Eqs. (10) and (11) can be combined with Eq. (9). With Eq. (11) for instance, one obtains

$$\Delta E^{ex} = (\gamma + \gamma' t)^{-1/2} \tag{12}$$

which has been found for Ag_{nc} in Ag^+ complex solutions [1].

2.3. Surface relaxation

In his derivation of growth laws Wagner [8] explicitly starts from particle shapes, which are already in the Gibbs–Wulff equilibrium. For an approximate estimation of surface energy differences, we may consider fcc crystals composed of only two types of planes (100) and (111), i.e. the cube, the octahedron and the mixed forms which are predominant for Cu [20]. The shape of the crystals can be described by normal distances of the planes from the centre, r_{100} and r_{111}, or by a single parameter α, defined in Eq. (13).

$$\alpha = r_{111}/r_{100}\sqrt{3}(\text{cube}) \geq \alpha \geq 1/\sqrt{3}(\text{octahedron}) \tag{13}$$

According to the simplest model [21], the surface energy per surface atom is the sum of the energies of the free bonds. The bond energy for closed-packed metals, ι, comes from the sublimation energy, $\Delta_s U$ (N_A: Avogadro number)

$$\psi = \Delta_s U / 6 N_A \tag{14}$$

The specific surface energies (σ_{100} and σ_{111}) are obtained by reference to the surface area using the atomic radius r_a

$$\sigma_{111} = \psi\sqrt{3}/2\, r_a^2 \tag{15a}$$

$$\sigma_{100} = \psi / r_a^2 \tag{15b}$$

Neglecting entropic and volume contributions ($G \cong U$), the molar excess Gibbs energy of the surface is written in the form of

$$\Delta G^{ex}_{GW} = (M\, \Delta_s H / N_A\, \rho\, r_a^2\, r_s)\{f(\alpha) + r_a\, k(\alpha)/r_s\} \tag{16}$$

(M: molar mass; ρ: density; r_s: radius of a sphere with identical volume).

The functions $f(\alpha)$ and $k(\alpha)$ contain geometrical terms for the calculation of the surface and of the edge length (see Appendix A). The expression in braces of Eq. (16) (see Fig. 1) exhibits a minimum at $\alpha = 0.145$ for $f(\alpha)$ (neglecting edge atoms) and a small shift of this minimum for decreasing crystal size. This minimum corresponds to the Gibbs–Wulff equilibrium shape with minimal surface energy.

With Eq. (16) the energetic difference between high (non-equilibrium) and low energy (relaxed) crystals and with Eq. (7) the excess EMF can be calculated. Taking the maximal differences on the ordinate of Fig. 1 between a macroscopic single crystal ($r_s = 1$ mm) and a nanocrystal ($r_s = 20$ nm), one obtains

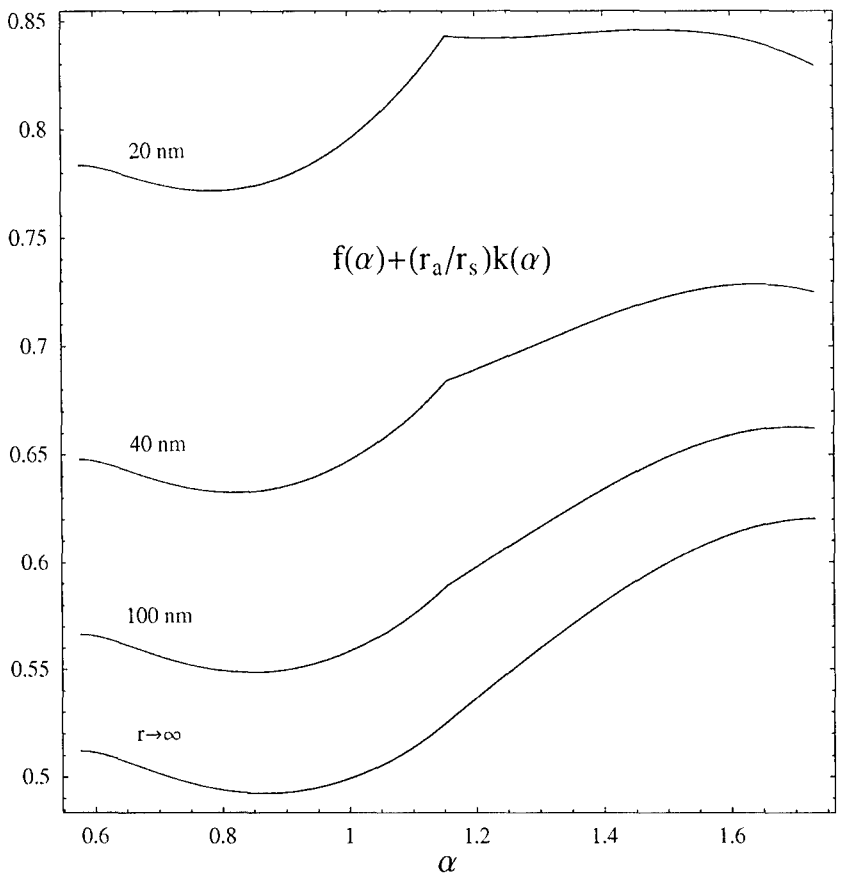

Fig. 1. Shape-dependent factor of molar Gibbs–Wulff energy ΔG^{ex}_{GW} (cf. Eq. (16)).

$\Delta U^{ex}_{GW}(1\text{ mm}) \approx 3\text{ mJ mol}^{-1}$ $\Delta U^{ex}_{GW}(20\text{ nm}) \approx 1\text{ kJ mol}^{-1}$
$\Delta E^{ex}_{GW} \approx 16\text{ nV}$ $\Delta E^{ex}_{GW} \approx 5\text{ mV}$

In principle these quantities are in a measurable range for nanocrystals, but they can rarely be distinguished from other excess energies.

Another interesting fact is that when edge energy is included, nanocrystals ($r_s = 20$ nm) with α values between $\sqrt{3}$ (cube) and $2/\sqrt{3}$ (cubooctahedron) have nearly constant surface energies and might be rather stable towards small fluctuations, whereas relaxation in the region $1/\sqrt{3}$ (octahedron)$\geq\alpha\geq 2/\sqrt{3}$ always ends in the minimum.

With the assumption that the relaxation kinetics $d\alpha/dt$ is driven by the gradient of ΔG^{ex}_{GW},

$$d\alpha/dt = -k'(\partial\Delta G^{ex}_{GW}(\alpha)/\partial\alpha)_{r_s=const} \quad (17)$$

it is easy to see that the rate law not only depends on the starting point α, but also on the size of r_s of the crystal. Relaxation of shapes between cube and cubooctahedron will only begin when $\partial\Delta G^{ex}_{GW}/\partial\alpha > 0$ i.e. when r_s will have grown over 20 nm. The important consequence is that relaxation is coupled with growing. Our treatment is simplified and only approximate, because for polycrystalline materials the shape equilibrium must in principle be discussed according to the Gibbs–Wulff–Kaischew theorem (c.f. [18] p. 152) and because in the solution the specific surface energy must be replaced by the interfacial energy. Nevertheless, one can conclude (even from Fig. 1) that there is no simple and characteristic time law for surface relaxation processes. The kinetics of a whole assembly of nanocrystals can not be predicted, which means that a direct experimental detection is not possible. Its

measurement would require that other equilibrium processes are excluded.

2.4. Electrochemistry of copper

Fig. 2 summarizes in a simplified scheme the processes occurring at a Cu electrode in a solution with Cu ions. It is well known that the Cu oxidation follows a two-step mechanism,

$$Cu^+ + e^- = Cu$$
$$E_I = E_I^0 + (RT/F)\ln[a(Cu^+)/a(Cu)] \quad (I)$$

$$Cu^{2+} + e^- = Cu^+$$
$$E_{II} = E_{II}^0 + (RT/F)\ln[a(Cu^{2+})/a(Cu^+)] \quad (II)$$

in which the exchange current of electrode reaction (I) is orders of magnitude higher than that of reaction (II). In the electrochemical equilibrium the electrode potentials E_I and E_{II} are equal, so that the chemical reaction of Cu^+ disproportionation (III) is also in equilibrium.

$$2Cu^+ = Cu^{2+} + Cu$$
$$K = a(Cu^{2+})\,a(Cu)/a(Cu^+)^2$$
$$= 2\times 10^6\,l\,mol^{-1} \quad (III)$$

This equilibrium can easily be disturbed by traces of oxygen, which oxidize Cu^+ (see Fig. 2). Then, the backward displacement of reaction (III) leads to a (positive) open circuit overvoltage [22], i.e. a corrosion potential is measured.

From electrode kinetics it has been concluded that in Eq. (I) Cu probably reacts mainly out of step positions (Cu_{step}) rather than as ad-atom (Cu_{ad}) [23]. Then it is easily understandable that the exchange current of reaction (I) has been found to be more than five times higher for Cu_{nc} than for Cu_{mc} [21], because the surface density of step atoms increases with decreasing crystal size. The electrode potential $E(Cu_{nc})$ is more negative than $E(Cu_{mc})$, so that ΔE^{ex} in Eq. (6) is positive. The Nernst equations (I) and (II) are applied by expressing ΔG^{ex} as

$$a^*(Cu) = a(Cu_{nc}) = \exp(-\Delta G^{ex}/RT) \quad (18)$$

using an activity $a^*>1$ for Cu_{nc}. In the local equilibrium between Cu_{nc} and the ions Cu^+ and Cu^{2+}, Eq. (II) shows that $a^*(Cu^+)$ in contact with Cu_{nc} will be enhanced, whereas $a(Cu^{2+})$ is normally fixed by the Cu(II) salt contained in the solution.

The local equilibrium will not be established if $a(Cu^+) \neq a^*(Cu^+)$, for instance in the presence of O_2 traces: $a(Cu^+)<a^*(Cu^+)$ (see above). The same inequality arises when normal Cu_{mc} and Cu_{nc} are present in the same solution. In the case of large surfaces of Cu_{mc} this metallic state will impose its $a(Cu^+)$ value on Cu_{nc}, so that reaction (III) is reversed, which means that Cu^{2+} oxidizes Cu_{nc}. Therefore, it is necessary to measure $E(Cu_{mc})$ and $E(Cu_{nc})$ separately against an inert reference electrode and to subtract the values according to Eq. (6). The converse situation must arise, when Cu_2O is added to an acid copper salt solution. The oxide dissolves and $a(Cu^+)$ reaches values even higher than in contact with Cu_{nc}. Then reaction (III) proceeds in the forward direction, meanwhile $E_I = E_{II}$ can no longer be valid. Reaction (I) will then determine the potential because of its higher exchange current.

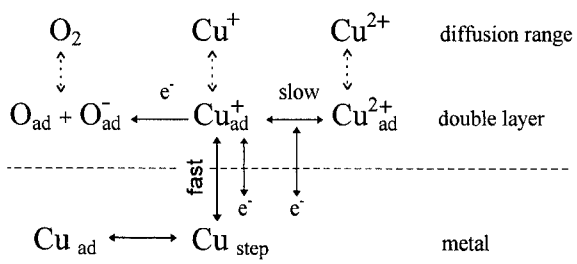

Fig. 2. Simplified scheme of the electrode processes on copper.

3. Experimental

The cells were totally made of glass, so that a N_2 gas flow which had only contact with glass could be passed through the cell or short-circuited by two three-way valves, completely sealing the cell under a standing N_2 atmosphere. The covers were designed for at least four electrodes, which could be immersed in or taken out of the cell solution. A magnetic device could be fixed to the cover, in order to pour small quantities of Cu_2O into the solution without opening the cell.

Cu_{nc} samples were prepared by inert-gas condensation [24]. Electrodes consisted of manually broken pieces of the Cu_{nc} tablets, coming from the preparation apparatus. Contacts to the electrode leads consisted of a conducting silver lacquer (Conrad) and an insulation of picein wax (Roth). Commercial Cu wire (99.99%), pre-treated by electrochemical polishing, was used for Cu_{mc} electrodes. Blank Pt electrodes were wires or small foil strips and cleaned in a H_2 flame. A $Hg/HgSO_4$ electrode with a diaphragm, but filled with the cell solution, was used as reference electrode. Its potential referred to NHE is not exactly known (~0.65 V), so our results are referred to this reference electrode, i.e. they are reported as the (negative) EMF values of the cell $Hg/HgSO_4$, H_2SO_4, $CuSO_4/Cu$.

The cell solutions were 0.5 M $CuSO_4$ in 0.5 M H_2SO_4 or 0.1 M $CuSO_4$ in 0.05 M H_2SO_4 (all analytical purity grade) in bidistilled water. For some purposes Cu powder (99.99%) was added to the solutions.

The grain size of the Cu_{nc} was determined from XRD (Siemens D500) patterns. The (111) and (222) reflections were used for the peak analysis. The area-weighted mean diameter and the average micro strain $\bar{\epsilon}$ were obtained by a Warren–Averbach evaluation, assuming spherical grain shape and log-normal size distribution [25]. The cell voltages were measured using computer-controlled electrometers (Bank, Prema).

4. Results and discussion

Three types of experiments were performed in order to study the changes in the EMF of cells with Cu_{nc} electrodes: They differ with respect to their closeness to the conditions of the local equilibrium.

When nitrogen (99.996%) was used for protection against oxygen, it was found that a small but reproducible corrosion of copper occurred, which shifted the electrical potentials of Cu_{mc} by about 10 mV in the positive direction, whereas Cu_{nc} is less affected, the effect decreasing with grain size e.g. with =4 nm no shift at all was detected. This behaviour is a consequence of the higher exchange current density of Cu_{nc} [22]. Two EMF curves of different Cu_{nc} samples under the slight O_2 corrosion (streaming N_2) were compared with the time law of Eq. (12) (Fig. 3). The comparison must be restricted

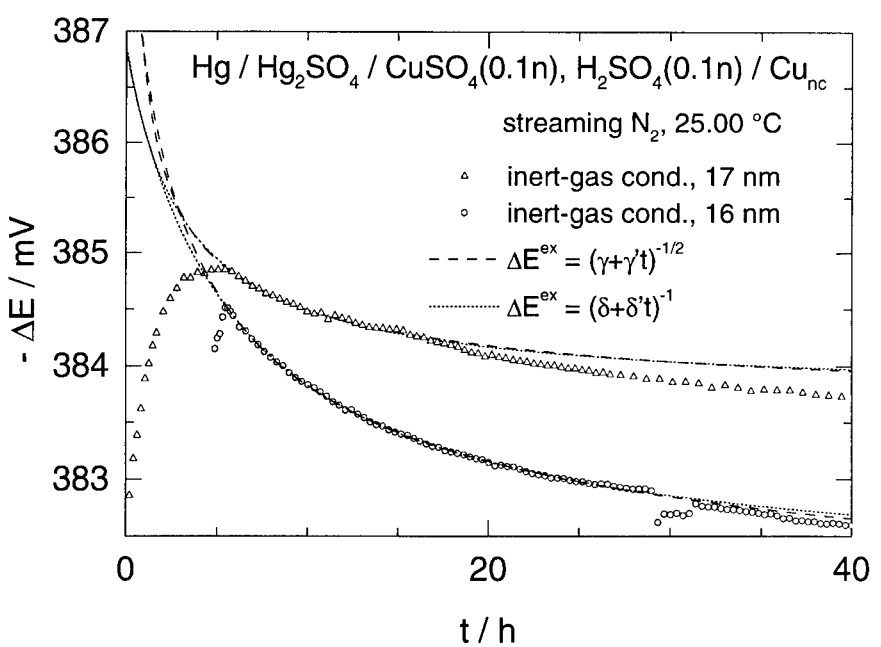

Fig. 3. Electrodes of nanocrystalline copper under slow corrosion by O_2.

to 5 h$<t<$15 h for sample 1, and to $t<$24 h for sample 2 because of some typical irregularities (cf. Section 5). The extrapolation with Eq. (12) to $t=0$ yields ΔE^{ex} values not fulfilling Eq. (9), which has been well corroborated with many Cu_{nc} samples of various sizes [3]. An extrapolation using the empirical law $\Delta E^{ex}=f(t^{-1})$ gives results which fit Eq. (9).

An example of the second type of experiments is shown in Fig. 4. Here the solution in the closed cell was completely freed from O_2 by Cu powder and the Cu_{nc} electrode was immersed thereafter. A comparatively fast change of the EMF was found with a very good global fulfillment of Eq. (12), although short regions of enhanced deviations occur (Section 5).

Traces of oxygen could also be completely removed over a long period by the action of the Cu_{mc} electrode itself (Fig. 5). The best proof of the absence of corrosion is the equality of the potential, measured at Cu_{mc}, and at Pt. When the Cu_{nc} electrode was dipped in the solution (tilting of the cell) and Cu_{mc} taken out of the solution, the potentials of Cu_{nc} (E_I) and Pt (E_{II}) decreased, but in a diverging manner. The explanation – according to the Nernst Eq. (I) E_I should increase with $a(Cu^+)$, when Cu_{mc} is exchanged by Cu_{nc} – will be given in Section 4.

Another obvious peculiarity is that during the first hour two different processes are occurring at the Cu_{nc} electrode, where the faster one produces a short minimum in the curve, which is reproducible within slight variations of shape. We were able to show that both effects were caused by the dissolution of the Cu_2O, which had formed at the surface of Cu_{nc} since the time of its preparation (see below).

When a small quantity of Cu_2O was added to the stirred O_2-free cell solution, the electrical potentials of Cu_{mc} and Pt electrodes changed significantly (Fig. 6). A sharp minimum appeared followed by a flat maximum and a rather slow decrease afterwards. A certain quantity of Cu_2O remains undissolved, mixed with Cu_{nc} nanocrystals ($\geq$20 nm). It has long been known, that Cu_2O reacts in sulphuric acid to Cu^{2+} ions and Cu_{nc} with intermediate formation of Cu^+ ions. However, the mechanism has never been studied in detail. From our experiments we deduce that Cu_{nc} forms at least partially at the metal surfaces of both electrodes, Cu_{mc} and Pt, but probably more rapidly at Cu_{mc}, which would explain the deviations in the time range 142.5 h$<t<$144 h. The size of these crystals just grown over the state of nuclei yields large ΔG^{ex}_{GT} and (negative) ΔE^{ex} values, but it

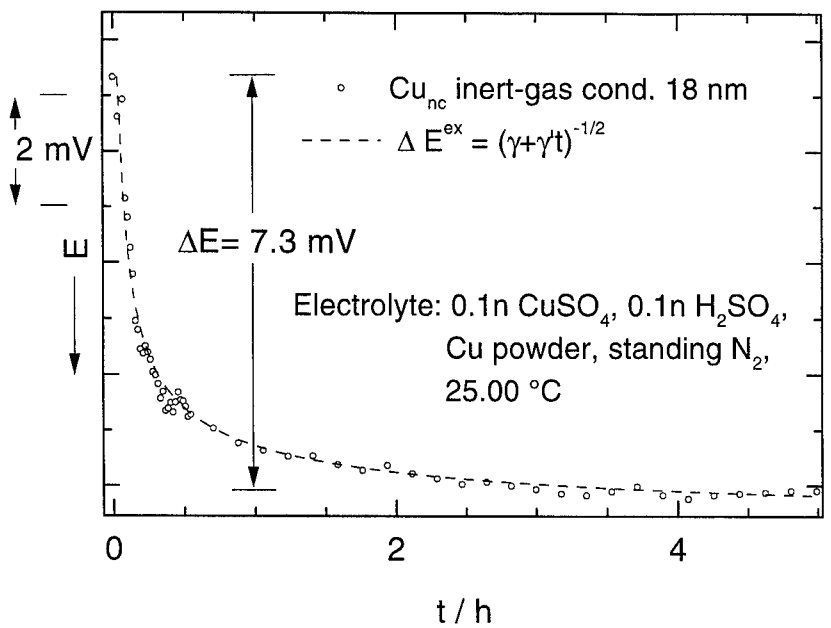

Fig. 4. Electrode of nanocrystalline copper corroded by Cu^{2+} ions.

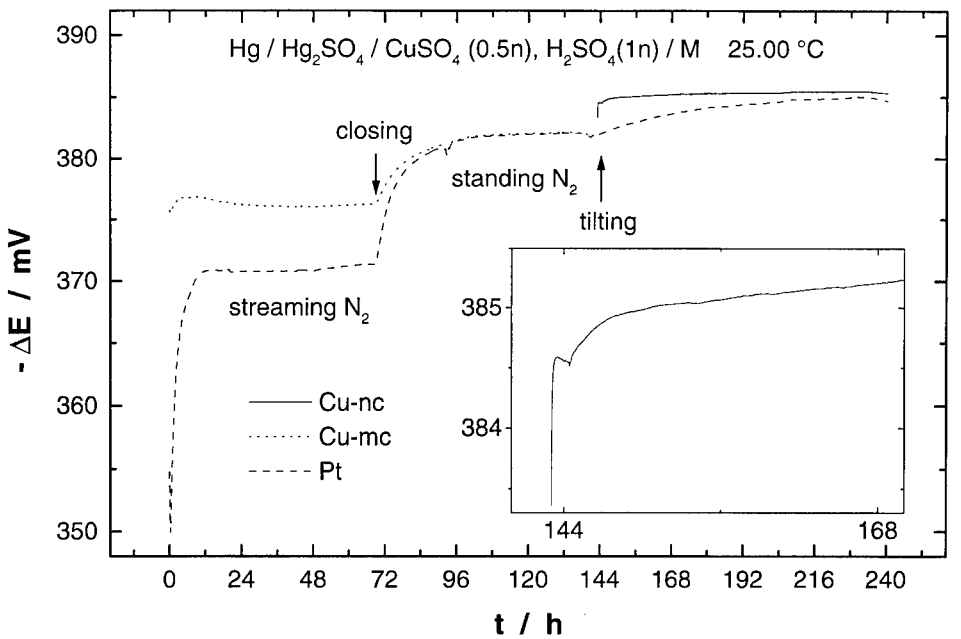

Fig. 5. Electrodes of Pt, micro- and nanocrystalline ($r=45$ nm) copper in a tiltable cell. N_2 contains 40 ppm O_2; in the closed cell O_2 is trapped by Cu_{mc}; by tilting Cu_{mc} is pulled out and Cu_{nc} dipped into the solution.

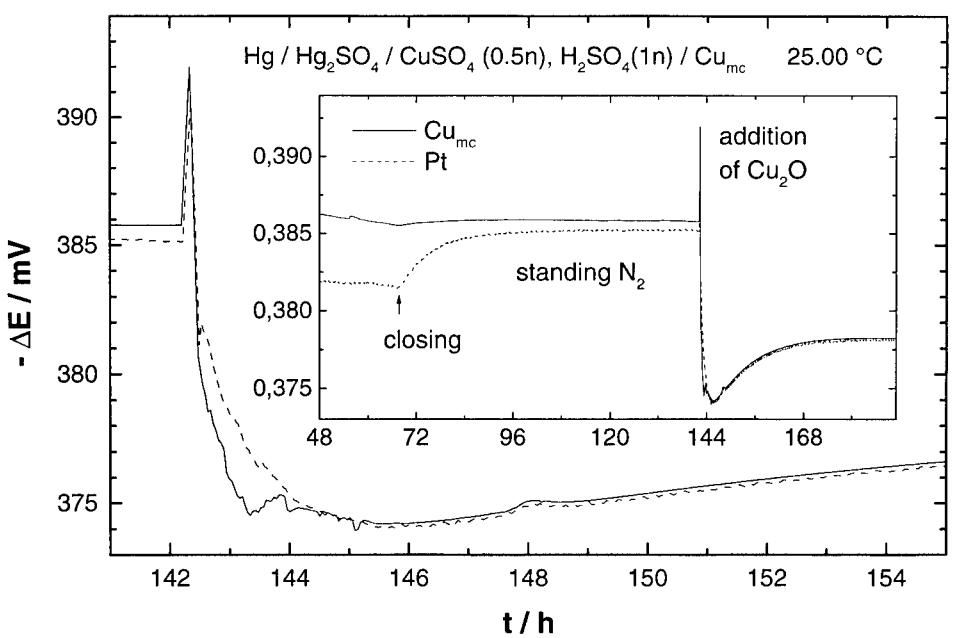

Fig. 6. Potentiometric study of the dissolution of 0.4 mg Cu_2O in 45 ml of the solution.

entails fast growth. The potential rises to a flat maximum determined by the superelevated Cu^+ ion concentration. The following decrease of ΔE^{ex} could be well described by a 1st order rate law in accordance with a catalytic decay of Cu^+ on the metallic surfaces. (Further EMF and kinetic studies on the Cu^+ disproportionation are underway). The same reaction order was found for the increase of the potential of the Pt electrode after the immersion of Cu_{nc} in Fig. 5. Obviously the small minimum in this Cu_{nc} curve is due to a slight reactive deposition of supplementary Cu_{nc} on Cu_{nc} and the following decrease of both potentials, of Cu_{nc} and Pt, by the Cu^+ diproportionation.

5. Conclusion

In the experiments without any corrosion, for which Fig. 6 gives an example, there is only one identifiable operative process: The initial dissolution of Cu_2O, which induces the decomposition of Cu^+. Over a period of nearly 100 h the Cu_{nc} curve shows no other marked phenomena than small fluctuation (<0.1 mV), best seen in the inlet of Fig. 6. No relaxation of any type can be observed. When slow corrosion processes are active, either by O_2 (Fig. 3) or by Cu^{2+} (Fig. 4), short positive (1 mV) deviations from the elsewhere smooth $E(t)$ courses appeared after irregular time intervals. Sometimes they were accompanied by similar features of the Pt potential (not shown in Figs. 4 and 5), which means that Cu_2O particles had been liberated in the nanocrystalline electrode, with a subsequent change of the Cu^+ concentration. The irregular course was only visible in the Cu_{nc} potential in few cases. Then it can be concluded that relaxation takes place, but until now no distinction between surface or strain relaxation is possible. These negative results are not in contrast to the theoretical considerations, which showed that no general time dependence and no prediction of the time of appearence can be expected for surface relaxation.

On the other hand, we demonstrated by this work that under total exclusion of O_2, which can be reached by trapping it within the cell, potentials of Cu_{mc} and Cu_{nc} can be measured with satisfactory precision. Therefore it would be possible and interesting to repeat some of the experiments with other types of Cu_{nc} (e.g. electrodeposition, ball-milling).

Acknowledgements

This work was supported by the Deutsche Forschungsgemeinschaft in the frame of SFB 277. We are thankful to Prof. Birringer and his group for preparing the nanocrystalline Cu samples.

Appendix A

The molar free surface energy ΔG^{ex}_{GW} is composed of the contributions from the two types (i) of surfaces $\sigma_i A_i(\alpha, r_s)$, where the total area A_i of the type i depends on the spherical shape α and the effective spherical radius r_s, and of the three types (j) of edges $\kappa_j L_j(\alpha, r_s)$, where κ_j stands for the specific edge energy ($\kappa_{111/100}$, $\kappa_{111/111}$, $\kappa_{100/100}$) and L_j for the total length of the edge type. After referring these contributions to the amount of the crystal (V: its volume) a transformation of Eq. (14) leads to Eq. (16),where $f(\alpha)$ and $k(\alpha)$ are given by Eq. (A.2) and Eq. (A.3).

$$\Delta G_{GW} = M\{\sum_i \sigma_i A_i(\alpha, r_s) + \sum_j \kappa_j L_j(\alpha, r_s)\}/V(r_s)\,\rho \tag{A.1}$$

$$f(\alpha) = \begin{cases} \dfrac{3^{1/3}}{4\pi^{1/3}} \dfrac{-5+23^{3/2}\alpha-3\alpha^2}{(-7+3^{5/2}\alpha-9\alpha^2+3^{1/2}\alpha^3)^{2/3}} & \sqrt{3} \geq \alpha \geq \dfrac{2}{\sqrt{3}} \\ \dfrac{3^{1/3}}{4\pi^{1/3}} \dfrac{-1=23^{1/2}\alpha}{(1-3^{3/2}\alpha+9\alpha-23^{1/2}\alpha^3)^{2/3}} & \dfrac{2}{\sqrt{3}} \geq \alpha \geq \dfrac{1}{\sqrt{3}} \end{cases} \tag{A.2}$$

$$k(\alpha) = \begin{cases} \dfrac{306^{1/2}\alpha}{(3^{3/2}\alpha^3-(3^{1/2}\alpha-1)^3)^{1/3}} & \sqrt{3} \geq \alpha \geq \dfrac{2}{\sqrt{3}} \\ \dfrac{962^{1/2}+186^{1/2}\alpha}{(6-(3-3^{1/2}\alpha)^3)^{1/3}} & \dfrac{2}{\sqrt{3}} \geq \alpha \geq \dfrac{1}{\sqrt{3}} \end{cases} \tag{A.3}$$

When Eq. (17) is valid for the relaxation kinetics one obtains $\alpha(t)$ by numerical integration of Eq. (A.4).

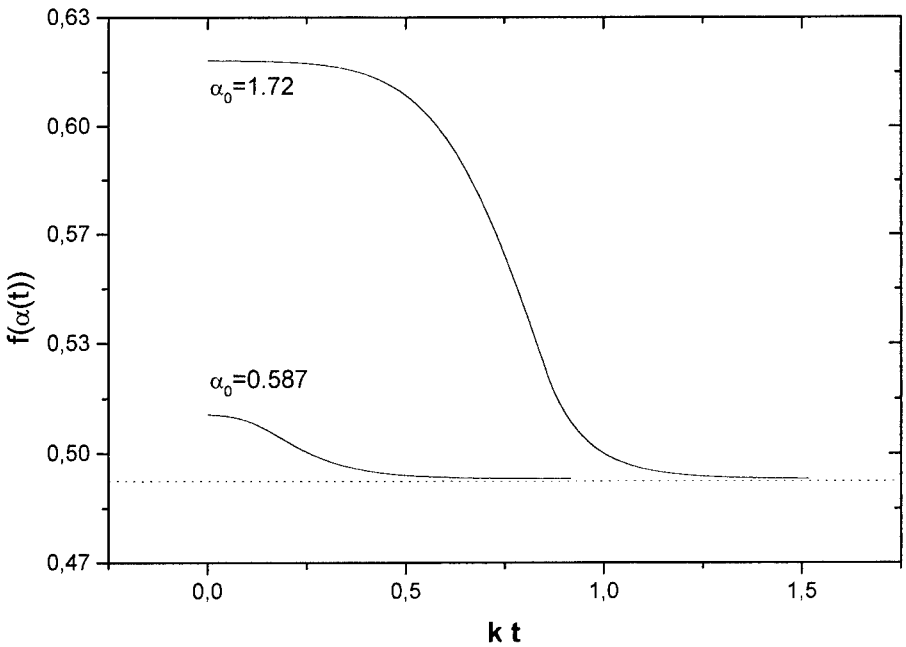

Fig. 7. Factor $f(\alpha(t))$ as a measure of surface energy in its time dependence; starting near cube: $\alpha_0 = 1.72$; starting near octahedron: $\alpha_0 = 0.587$.

$$d\alpha/dt = -k' (\partial \Delta G_s(\alpha)/\partial\alpha)_{r_s=\text{const}} = -k\, \partial\{f(\alpha) + r_a\, k(\alpha)/r_s\}/\partial\alpha \qquad \text{(A.4)}$$

$$\int_{\alpha_0}^{\alpha(t)} \frac{d\alpha}{\partial\{f(\alpha) + r_a k(\alpha)/r_s\}/\partial\alpha} = -kt \qquad \text{(A.5)}$$

Then $\Delta G^{ex}_{GW}(t)$ can be calculated. As an example we plot in Fig. 7 the factor $f(\alpha(t))$, which determines the rate for $r_s > 100$ nm.

References

[1] S. Villain, P. Knauth, G. Schwitzgebel, Phys. Chem. B101 (1997) 7452.
[2] P. Knauth, G. Schwitzgebel, A. Tschöpe, S. Villain, J. Solid State Chem. 140 (1998) 295.
[3] U. Heim, G. Schwitzgebel, Nanostruct. Mater. 12 (1999) 19.
[4] G. Schwitzgebel, R. Mildenberger, Ber. Bunsenges. Phys. Chem. 101 (1997) 1742.
[5] E. Budevski, V. Bostanov, Electrochim. Acta 9 (1964) 477.
[6] J. Rupp, R. Birringer, Phys. Rev. B36 (1987) 7888.
[7] K.-St. Werkmeister, F. Rullang, M. Koch, M. Heyer, G. Schwitzgebel, Nanostruct. Mater. 12 (1999) 229.
[8] C. Wagner, Z. Elektrochem. 65 (1961) 581.
[9] D. Henning, K.G. Weil, Ber. Bunsenges. Phys. Chem. 82 (1978) 265.
[10] F. Gärtner, R. Bormann, R. Birringer, A. Tschöpe, Scripta Mater. 35 (1996) 805.
[11] U. Heim, Thesis, Saarbrücken, 2000.
[12] C.P. Gräf, Diploma Work, Saarbrücken, 1998.
[13] G. Schwitzgebel, Z. phys. Chem. NF 95 (1975) 15.
[14] G.B. Rais, M.J. Bromberg, E.M. Gugel, Fizika Tverdogo Tela 8 (1966) 3700.
[15] D. Lewis, C.E. Pearce, Electrochim. Acta 16 (1971) 747.
[16] L.E. Chen, F. Spaepen, J. Appl. Phys. 69 (1991) 689.
[17] F.J. Humphreys, M. Hatherly, Recrystallization and Related Annealing Phenomena, Pergamon (Elsevier Science Ltd), Oxford, 1996.
[18] E. Budevski, G. Staikov, W.J. Lorenz, Electrochemical Phase Formation and Growth, Wiley, Weinheim-New York, 1996.
[19] B.K. Chakraverty, J. Phys. Chem. Solids 28 (1967) 2401.
[20] B. Honigmann, Gleichgewichts- und Wachstumsformen von Kristallen, Steinkopf Verlag, Darmstadt, 1958.
[21] W. Romanowski, Surface Science 18 (1969) 373.
[22] C.P. Gräf, U. Heim, G. Schwitzgebel, in preparation
[23] A. De Agostini, E. Schmidt, W.J. Lorenz, Electrochim. Acta 34 (1989) 1243.
[24] H. Gleiter, Phase Transition 24 (1990) 15.
[25] H. Natter, R. Hempelmann, Ber. Bunsenges. Phys. Chem. 100 (1996) 55.